Energy dependence of two-nucleon pion absorption on ^{16}O

S. D. Hyman,[a] D. J. Mack,[b] P. G. Roos, H. Breuer, N. S. Chant, F. Khazaie,[c] B. G. Ritchie,[d] and J. D. Silk[e]
Department of Physics, University of Maryland, College Park, Maryland 20742

G. S. Kyle
Department of Physics, New Mexico State University, Las Cruces, New Mexico 88003

P. A. Amaudruz,[f] Th. S. Bauer,[g] C. H. Q. Ingram, D. Renker, R. A. Schumacher,[h] and U. Sennhauser[i]
Paul Scherrer Institute, CH-5234, Villigen, Switzerland

W. J. Burger[j]
Massachusetts Institute Technology, Bates Laboratory, Middleton, Massachusetts 01949
(Received 12 October 1992)

Inclusive $^{16}O(\pi^+, p)$ and exclusive $^{16}O(\pi^+, 2p)$ data are presented for 115 MeV and 165 MeV pions. Using a combination of distorted-wave impulse approximation (DWIA) calculations for two-nucleon absorption and phase space simulations for more complicated processes, the data are fit and the total direct two-nucleon absorption cross sections are extracted. These cross sections fall faster with energy than $\pi^+ d \rightarrow pp$. The DWIA calculations were used to calculate the effects of final state interactions (FSI). After correcting for FSI, the two-nucleon absorption process is found to dominate at 115 MeV, becoming less important as the incident energy increases to 165 MeV. The decrease with energy in the two-nucleon fraction of the total absorption cross section is found to be in remarkably good agreement with theoretical predictions.

PACS number(s): 25.80.Ls

I. INTRODUCTION

Pion absorption by nuclei has received a great deal of attention over the past few years. Many of these works address the relative roles of absorption by two nucleons in nuclei versus absorption by three or more nucleons in some direct process. Most experiments have concentrated on the measurement of two-particle final states, primarily $(\pi^+, 2p)$, and have attempted to extract the two-nucleon absorption strength. By comparing these extracted two-nucleon absorption cross sections to the total absorption cross section, multinucleon absorption probabilities were inferred. The results vary greatly, with values for the percentage of two-nucleon absorption ranging from roughly 25% to 80% of the total absorption cross section depending on target, energy, and method of analysis. In addition to experimental difficulties related to their coverage of phase space, the extraction of the two-nucleon absorption cross section is greatly hampered by our lack of understanding of the effects of initial state and final state interactions (ISI's and FSI's). These processes cause a large fraction of the two-nucleon absorption yield to be redistributed into other kinematic regions, making it difficult to identify.

More recent experiments have detected multinucleon final states. These experiments seem to indicate that the role of multinucleon absorption in light nuclei ($A < 12$) is relatively small (<30%) [1–4], a number consistent with the higher two-nucleon absorption percentages men-

[a]Present address: Sweet Briar College, Sweet Briar, VA 24595.
[b]Present address: CEBAF, Newport News, VA 23606.
[c]Present address: University of Liverpool, England.
[d]Present address: Arizona State University, Tempe, AZ 85287.
[e]Present address: IDA, Alexandria, VA 22311.
[f]Present address: TRIUMF, Vancouver, B.C., V6T 2A3 Canada.
[g]Present address: Physics Laboratory, Utrecht University, 3508 TA Utrecht, The Netherlands.
[h]Present address: Carnegie-Mellon University, Pittsburgh, PA 15213.
[i]Present address: EMPA, Dübendorf, Switzerland.
[j]Present address: University of Geneva, Geneva, Switzerland.

tioned above. However, these results were obtained either with very large extrapolations (10^4) of the measured data using a phase space model or have little granularity so that the separation of direct two-nucleon absorption from ISI's and FSI's using kinematic variables is essentially impossible. Until such time as more detailed multinucleon final state data become available, detailed absorption studies detecting two nucleons in the final state can provide quantitative information on the two-nucleon absorption strength, and by inference the fraction of more complicated processes present in pion absorption.

In previous papers we presented results for $^{16}O(\pi^+, 2p)$ at 115 MeV [5] and preliminary results for 165 MeV [6]. These analyses indicated a dominance of the two-nucleon absorption mechanism at 115 MeV, approximately 75% of the total absorption cross section, decreasing to perhaps 50% at 165 MeV. Both results include the contributions from FSI's, but exclude contributions from ISI's. In this paper we present a careful and consistent analysis of the data for the two incident energies to illuminate the energy dependence of the $^{16}O(\pi^+, 2p)$ reaction. This consistent analysis is carried out for both the exclusive $^{16}O(\pi^+, 2p)$ and inclusive $^{16}O(\pi^+, p)$ data. In particular, whereas we have used a number of methods to analyze background data in the past, we now employ one technique at both energies.

After a brief review of the experiment (Sec. II), we present in Sec. III the data showing the reduction in cross section with increasing energy for regions dominated by two-nucleon absorption. This is true of both the inclusive and the exclusive cross sections. In Sec. IV we discuss the theoretical analyses used. Distorted wave impulse approximation (DWIA) calculations are used to describe the two-nucleon absorption component and to extrapolate the data into the unmeasured regions. The DWIA calculations are also used to calculate the contributions to the cross section from FSI's, a result which is tested by comparing suitable DWIA calculations with the inclusive data. Phase space calculations are used to simulate the multinucleon processes which provide a background underlying the two-nucleon absorption yield. In Sec. V we present the extracted two-nucleon absorption cross sections, both with and without corrections for FSI's. The final section (Sec. VI) summarizes the present results.

II. EXPERIMENTAL DETAILS

The experiment has been discussed in detail in Refs. [5, 7, 8]. We therefore provide only a brief review of the experimental setup here. The measurements were carried out at the $\pi M1$ channel of the Paul Scherrer Institute. Pion beams of 115 MeV and 165 MeV with fluxes ranging from 3×10^6 to 9×10^6 π^+/sec were incident upon a 4-mm-thick H_2O target. A schematic diagram of the experimental layout was presented in Ref. [5]. The incident pion beam momentum and intensity were measured with a 16-element hodoscope at the intermediate focus of the $\pi M1$ channel and an in-beam scintillator. The hodoscope permitted a measurement of the incident pion momentum to within approximately 0.25%, as well as the removal of almost all events with more than one pion in the rf microburst. The combination of an electrostatic separator in the channel and time-of-flight and in-beam scintillator pulse-height measurements using the primary proton beam rf structure kept proton and muon contamination of the pion beam to less than 1%.

Protons emerging from the $^{16}O(\pi^+, 2p)$ reaction were detected with the SUSI magnetic spectrometer [9] with a solid angle of approximately 13 msr in coincidence with a large (approximately 600 msr) multiwire proportional chamber and plastic scintillator array. The combined system provided an excitation energy resolution of better than 6 MeV in the residual ^{14}N nucleus. Data were taken for five SUSI magnetic field settings covering proton energies from approximately 50 MeV to 230 MeV. The MWPC/plastic scintillator array measured protons with energies from 35 MeV (due primarily to the thickness of the ΔE detector) up to the maximum kinematically possible in the present experiment.

At the two energies both inclusive $^{16}O(\pi^+, p)$ and exclusive $^{16}O(\pi^+, 2p)$ data were obtained for five angle settings of the spectrometer. These were $\theta_1 = 30°$, $50°$, $78°(76°)$, $107.5°(105°)$, and $133°(132°)$ where the numbers in parentheses represent the slightly different angles used in the 165 MeV measurements. For each spectrometer angle coincident data were taken with the large scintillator array centered at an angle on the opposite side of the beam conjugate to the spectrometer angle for the $\pi^+ d \rightarrow pp$ reaction. In the following the angle of the second proton is defined in terms of a detector angle θ_2, measured in the reaction plane defined by the incoming pion and first proton, and an angle of noncoplanarity β_2, measured in a plane perpendicular to the reaction plane. In addition to the central setting of the scintillator array, whenever physically possible two additional overlapping angle settings of the array were taken to provide in-plane angular coverage of approximately $\Delta\theta_2 = \pm 58°$. For all settings the scintillator array covered an out-of-plane angular range of $\Delta\beta_2 = \pm 23°$.

Cross sections were determined using the measured pion flux, target thickness, solid angles, and measured efficiencies. These values were checked with measurements of elastic π^+ scattering from ^1H and ^{16}O and with numerous measurements, both in singles and coincidence, of $\pi^+ d \rightarrow pp$ using a 4 mm D_2O target. Based on the consistency of these various measurements, we estimate the systematic uncertainty in cross sections to range from 8% to 10% depending on the type of data.

III. EXPERIMENTAL DATA

In this section we first examine the inclusive $^{16}O(\pi^+, p)$ data. In Fig. 1 we present the cross sections at the two incident energies. At both forward and backward angles one observes a clear signature of two-nucleon absorption with a broad maximum peaking nearly at the proton momentum corresponding to $\pi^+ d \rightarrow pp$. At the middle angle $78°(76°)$ no clear peak exists. This angle corresponds to 90° in the c.m. system for $\pi^+ d \rightarrow pp$, the angle at which the absorption cross section is a minimum, and one would expect contributions from other more complicated processes to be relatively more important. At the

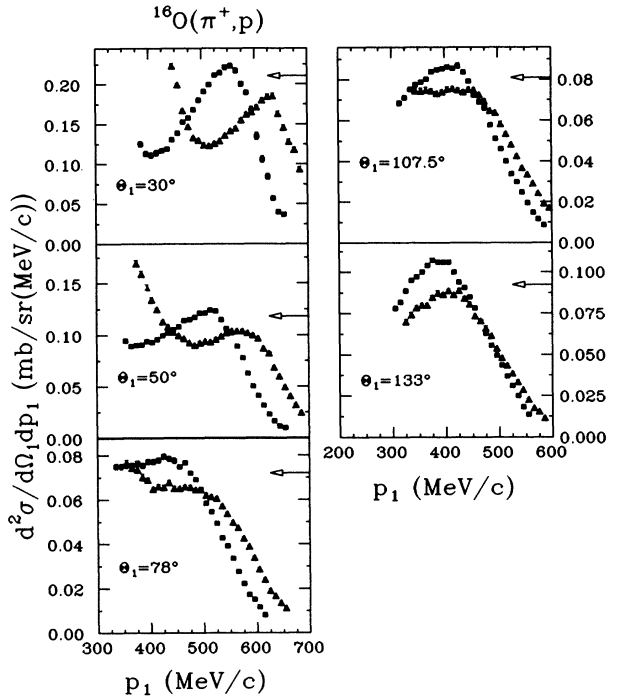

FIG. 1. Inclusive $^{16}O(\pi^+,p)$ cross sections for incident pion energies of 115 MeV (□) and 165 MeV (△). The statistical errors are smaller than the symbols. The angle θ_1 of the proton detected in the spectrometer is indicated for E_π = 115 MeV. The horizontal arrows indicate the value of the peak cross section expected at 165 MeV if one scales the 115 MeV cross section by the $\pi^+d \rightarrow pp$ cross section.

most forward angle of 30° the cross section rises at low momenta, indicating contributions from quasifree knockout $^{16}O(\pi^+,\pi^+p)$. Although it is kinematically possible to have quasifree proton knockout contributions near the two-nucleon absorption maxima, these should be negligible since they require protons bound in the nucleus with momenta in excess of 500 MeV/c.

When the abscissa is adjusted for the differences in the available energy, the shape of the data near the peak is very nearly the same at the two incident energies. Assuming that a major component of the maxima in these inclusive spectra arises from two-nucleon absorption, we would expect the energy dependence of the cross section to be similar to that of $\pi^+d \rightarrow pp$. This would be true particularly at the most forward angles where the two-nucleon absorption cross section is largest compared to the background data arising from other processes. The horizontal arrows in Fig. 1 represent a scaling of the peak in the 115 MeV inclusive cross sections to 165 MeV using the energy dependence of the $\pi^+d \rightarrow pp$ differential cross section at each angle. Even at 30° the peak of the inclusive cross section falls more rapidly than expected based on this naive model.

In Fig. 2 we present typical excitation energy spectra for the exclusive $^{16}O(\pi^+,2p)$ reaction. Data are presented for two angle pairs, one for the quasifree angle pair (the angle pair corresponding to the absorption on a deuteron at rest in the target nucleus which is essentially the angle pair for $\pi^+d \rightarrow pp$) and a second pair far from this quasifree condition. One observes the strong population of the low excitation energy region for the quasifree angle pair. Based on our previous work we have chosen to divide the data into the excitation energy bins 0–20 MeV (primarily absorption on a pair of 1p-shell nucleons in the nucleus) and 20–70 MeV (a combination of 1p-1s shell nucleon absorption and more complicated process such as multinucleon absorption). The data for the high excitation energy region, 70–140 MeV, generally follow a three-nucleon phase space distribution, and are therefore unlikely to contain any direct two-nucleon absorption contributions. Above 140 MeV excitation energy, pions are energetically permitted in the final state and therefore need not to have been absorbed. These data were not analyzed. For the 165 MeV data we have further subdivided the 20–70 MeV range into two energy regions of equal size.

In the previous papers two basic types of data were presented for each excitation energy region: (a) a momentum sharing distribution for each spectrometer angle

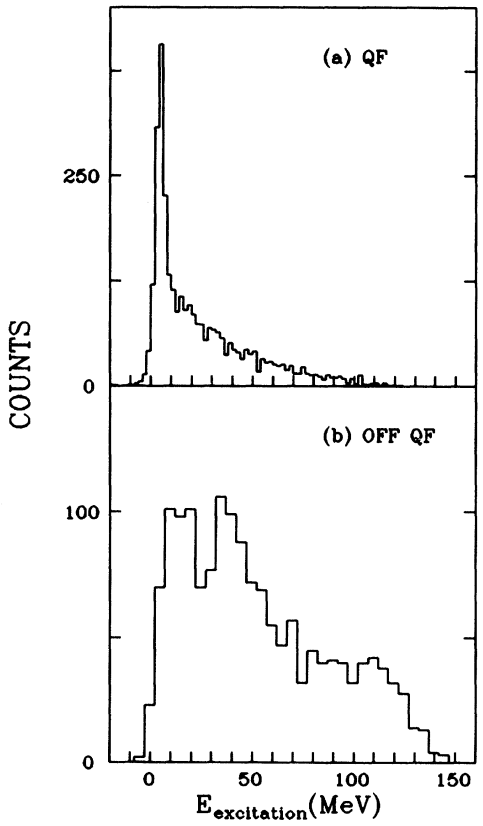

FIG. 2. Excitation energy spectra for $^{16}O(\pi^+,2p)$ at 165 MeV. Panel (a) corresponds to proton angles centered at θ_1 = 50°, θ_2 = −105°, an angle pair for which low recoil momentum is predominant. Panel (b) corresponds to angles centered at θ_1 = 50°, θ_2 = −87.5°, an angle pair such that higher recoil momenta (>100 MeV/c) are emphasized.

integrated over the central setting of the scintillator array and (b) for each spectrometer angle an angular correlation with the scintillator array integrated over the spectrometer momentum. In the present paper we will use only the momentum sharing distributions $d^2\sigma/d\Omega_1 dp_1$. These consist of data integrated over the full solid angle of the scintillator array positioned at the central quasifree setting [$\theta_2 = \theta_2(qf) \pm 25°$, $\beta_2 = \pm 23.7°$] and displayed as a function of proton (spectrometer) momentum.

In Fig. 3 the momentum sharing distributions for the 0–20 MeV excitation energy range for both incident energies are presented. The upward arrows in the 30° and 50° panels mark the onset of the plastic scintillator threshold for the 115 MeV data; above the arrows the cross sections are underrepresented. Because of the greater available energy, the threshold did not affect the 165 MeV data in this excitation energy range. As in Fig. 1, the horizontal arrow represents expectations based on a naive scaling of the peak cross sections at 115 MeV by the $\pi^+ d \rightarrow pp$

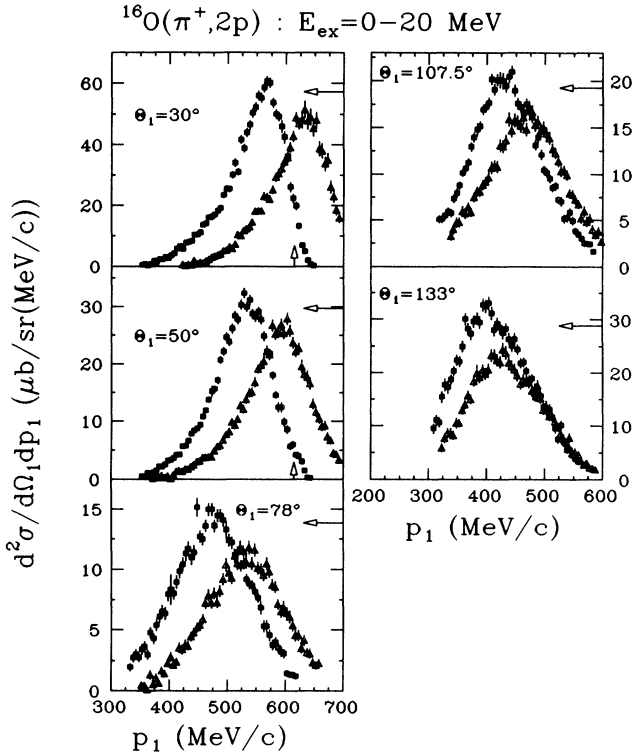

FIG. 3. Momentum sharing distributions for the $^{16}O(\pi^+, 2p)^{14}N$ reaction at pion incident energies of 115 MeV (□) and 165 MeV (△) and with 0–20 MeV excitation energy in the residual nucleus ^{14}N. One proton was detected with the SUSI spectrometer set at θ_1. The coincident proton was detected with the large plastic scintillator array (~600 msr) centered at the conjugate angle for the $\pi^+ d \rightarrow pp$ reaction. The horizontal arrows indicate the value of the peak cross section expected at 165 MeV if one scales the 115 MeV peak cross section by the $\pi^+ d \rightarrow pp$ cross section. The upward arrows indicate the onset of the plastic scintillator threshold. The 115 MeV data above this point represent lower limits.

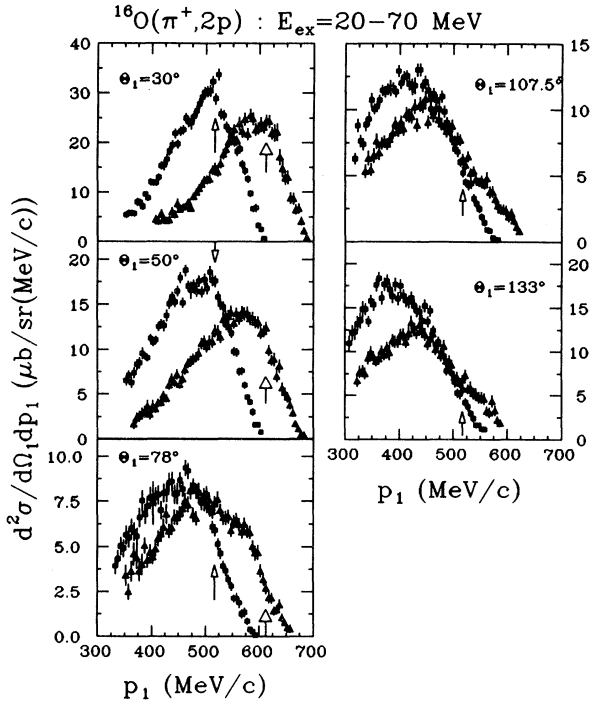

FIG. 4. Momentum sharing distributions for the $^{16}O(\pi^+, 2p)^{14}N$ reaction at pion incident energies of 115 MeV (□) and 165 MeV (△) and with 20–70 MeV excitation energy in the residual nucleus ^{14}N. One proton was detected with the SUSI spectrometer set at θ_1. The coincident proton was detected with the large scintillator array (~600 msr) centered at the conjugate angle for the $\pi^+ d \rightarrow pp$ reaction. The 115 (165) MeV data above the small (large) arrows represent lower limits due to the onset of the plastic scintillator threshold.

cross section. Again one observes that the cross sections drop more rapidly than predicted by this model. Also, as with the inclusive data, the shapes are essentially the same. Similar results for the 20–70 MeV excitation energy range are presented in Fig. 4 with similar conclusions. Note that in this higher excitation energy range the 165 MeV data are affected by the plastic scintillator threshold.

IV. THEORETICAL ANALYSIS

The extraction of the two-nucleon absorption cross section was carried out with the aid of two theoretical models. Direct two-nucleon absorption was modeled using a distorted-wave impulse approximation (DWIA) treatment of quasideuteron absorption. This model was also used to calculate the magnitude of the FSI. The underlying "backgrounds" from multinucleon processes, whether arising from multinucleon absorption, FSI's, or ISI's, were modeled with a Monte Carlo simulation of phase space. The incoherent sum of the two calculations was then fit to the data in order to extract the total two-nucleon yield.

A. DWIA calculations

The experimental data have been compared to factorized DWIA calculations assuming absorption on a quasideuteron in the nucleus. The theoretical formalism has been presented in Refs. [10] and [11] and details of the specific calculations undertaken here are discussed in Refs. [5] and [12]. In brief, the triple differential cross section for $A(\pi^+, 2p)B$ to a specific final state in nucleus B with angular momentum transfer L (z-projection Λ) is written as

$$\frac{d^3\sigma}{d\Omega_1 d\Omega_2 dE_1} = KF\frac{d\sigma}{d\Omega}\sum_{\Lambda} \mid T_{BA}^{L\Lambda} \mid^2, \quad (1)$$

with

$$T_{BA}^{L\Lambda} = \frac{1}{(2L+1)^{1/2}} \int \chi_{p_1 B}^{(-)^*}(\mathbf{k}_{p_1 B}, \mathbf{r}) \chi_{p_2 B}^{(-)^*}(\mathbf{k}_{p_2 B}, \mathbf{r}) \times \chi_{\pi A}^{(+)}\left(\mathbf{k}_{\pi A}, \frac{B}{A}\mathbf{r}\right) \phi_{L\Lambda}(\mathbf{r}) d^3 r. \quad (2)$$

In Eq. (1) the quantity KF represents a known kinematic factor and $d\sigma/d\Omega$ represents the off-shell πNN vertex. The amplitude $T_{BA}^{L\Lambda}$ contains the distorted waves χ to describe the incoming pion and outgoing protons. These are calculated using phenomenological optical model potentials. The amplitude also contains a microscopic form factor $\phi_{L\Lambda}$, the coordinate space wave function of the center-of-mass motion of the $^3S_1$ pair in the nucleus.

In the present calculations we have made three changes in comparison to the previous calculations of Refs. [5] and [12]. First, we have taken $d\sigma/d\Omega$ to be the on-shell $\pi^+ d \rightarrow pp$ cross section [13] at an angle and energy corresponding to the initial state of the pion-quasideuteron system (initial energy prescription). This particular prescription was chosen over others (e.g., the final energy prescription used in Refs. [5] and [12]), because it provides a somewhat better description of the energy dependence of the ^{6}Li$(\pi^+, 2p)$ data of Zhang [14] over the energy range 115–220 MeV. This is also true for the present ^{16}O$(\pi^+, 2p)$ data. Use of the final energy prescription can lead to discrepancies as large as 30%.

Second, we have employed two-nucleon sum rules [11], thereby requiring calculations for fewer nuclear states than in our past analyses. To accomplish this, we have assumed a closed-shell ^{16}O target nucleus and, furthermore, that the 0–20 MeV region exhausts the $(1p)^2$ strength (this is true for the wave functions of Cohen and Kurath [15]). These assumptions permit us to use sum rules for the $L = 0$ and $L = 2$ strength, ignoring small effects arising from the Q-value differences of the actual nuclear states. The sum rule has the added benefit that the effective tensor polarization of the bound deuteron due to the reaction [16] does not affect the sum, and therefore the factorization of the two-body cross section in this model is exact. In a similar fashion we assumed that the 20–70 MeV excitation energy region contains the summed $1s$-$1p$ and $(1s)^2$ strength. Support for this assumption has been presented in Refs. [5] and [6]. Therefore, sum rules could be applied to the $L = 1$ $(1s, 1p)$ and $L = 0$ $(1s^2)$ cross sections in this region.

For the 0–20 MeV $(1p^2)$ region, and using the sum rule, we consider effectively only two states. One state is reached by the transfer of an $L = 0$ deuteron, and the wave function $\phi_{L\Lambda}$ is normalized to the sum rule limit for the three possible 1^+ states in ^{14}N. [In a harmonic oscillator shell model basis the wave function would be normalized to give approximately 1.5 deuterons, this corresponding to the number of $^3S_1$ $n-p$ pairs in $(1p)^2$ with zero oscillator quanta in the relative motion wave function.] The second state is reached by the transfer of an $L = 2$ deuteron and normalized to the $L = 2$ sum rule limit for the 1^+, 2^+, and 3^+ states in ^{14}N (approximately 7.5 deuterons in the harmonic oscillator shell model basis). For the 20–70 MeV region in principle we have both $L = 1$ and $L = 0$ quasideuterons. However, using an oscillator shell model sum rule we have approximately 12.0 $(1s$-$1p)$ $L = 1$ quasideuterons and only 3.0 $(1s)^2$ $L = 0$ quasideuterons. In addition, the shape differences between $L = 0$ and $L = 1$ DWIA calculations for this excitation energy region are less pronounced. Therefore, to simplify the calculations we have carried out calculations for only $(1s$-$1p)$ $L = 1$. DWIA calculations were then carried out for the three configurations discussed above.

The third change with respect to our previous DWIA calculations is our choice of optical model potentials. For the outgoing protons we have used, as before, the global proton optical model potential of Nadasen *et al.* [17]. The pion potential presents more difficulty. No global fits to pion data exist above 80 MeV. In our previous analyses of these data we chose a low energy pion potential due to Amman *et al.* [18] for the 115 MeV calculations which is not applicable at 165 MeV. In the present paper a primary interest lies in the energy dependence of pion absorption. We therefore decided to generate a consistent energy-dependent pion potential for the two energies. Fortunately elastic scattering data exist at approximately the two energies of our pion absorption experiment [9].

The optical model analysis of the elastic scattering data was carried out with the code FITPI [19]. Since this is purely a phenomenological analysis, a simple Kisslinger-type potential, without the pion-nucleon angle transformation, was used. Initially, geometrical parameters were taken from electron scattering, and the strengths of the potential were varied to fit the data. However, to obtain a good fit some variation of the geometry was required (approximately a 5% reduction in radius and 15% reduction in diffuseness). The strengths were adjusted until good fits were achieved at both energies with a common geometry. The resultant fits and parameters (labeled FG) are presented in Fig. 5 and Table I, respectively.

Other parametrizations of the potential were tried to determine the sensitivity of the DWIA calculations to the choice of optical model potential. At the lower energy a Michigan State University (MSU) type potential [20] was fitted to the data [21]. This is a more complicated potential with many more parameters. These parameters were varied to fit the data, and the results are also shown in

TABLE I. Optical model parameters for pion elastic scattering from ^{16}O. Potential form: $V_N(r) = -Ak^2 b_0 \rho(r) + Ab_1 \nabla \cdot \rho \nabla$, where Fermi is given by $\rho_0/(1+e^{(R-r)/a})$ and harmonic oscillator by $\rho_0 \left[1 + \left(\frac{r-2}{3}\right)\left(\frac{r}{\alpha}\right)^2\right] e^{-r^2/\alpha^2}$.

Potential(density)	T_π (MeV)	R or α (fm)	a (fm)	Reb_0	Im b_0	Re b_1	Im b_1
FG (Fermi)	114.4	2.50	0.432	−2.40	−0.07	9.53	3.04
FG (Fermi)	162.6	2.50	0.432	0.25	−0.35	6.86	6.16
CM (harmonic oscillator)	114.4	1.769		−1.20	−1.55	6.69	2.22
CH (harmonic oscillator)	162.6	1.769		−0.76	0.42	7.21	2.45

Fig. 5. At the higher energy we tried the Cottingame-Holtkamp (CH) potential [22], the result of which is also shown in Fig. 5. Typical DWIA calculations using all of these potentials are shown in Fig. 6. DWIA calculations for other angles exhibit similar variations. For these choices of potential, all of which provide reasonably good fits to the elastic scattering data, the changes in the DWIA cross sections are small. For completeness we have also included in Fig. 6 calculations at 115 MeV using the Carnegie-Mellon (CM) potential of Amman *et al.* [18], the potential used in the previous analyses [5, 12]. This potential provides a poor fit to the 114.4 MeV elastic scattering data (see Fig. 5). The DWIA cross sections with this potential differ primarily in magnitude, although some shape differences are evident. In the remainder of the paper all DWIA calculations use our fitted pion potential. The other input is as discussed above.

The DWIA formalism contains various approximations which have been discussed in some detail in Refs. [11, 16]. Comparisons to experimental data for ^{16}O$(\pi^+, 2p)$ [5, 12] have shown that such calculations reproduce the dependence of the reaction on a variety of kinematic variables quite well. The one major discrepancy lies in the overall magnitude of the calculations. In the comparisons made to ^{16}O$(\pi^+, 2p)^{14}$N, the DWIA calculations appear to be about a factor of 3–10 smaller than the data, depending on the nuclear states. The origins of the discrepancies remain to be understood, whether they

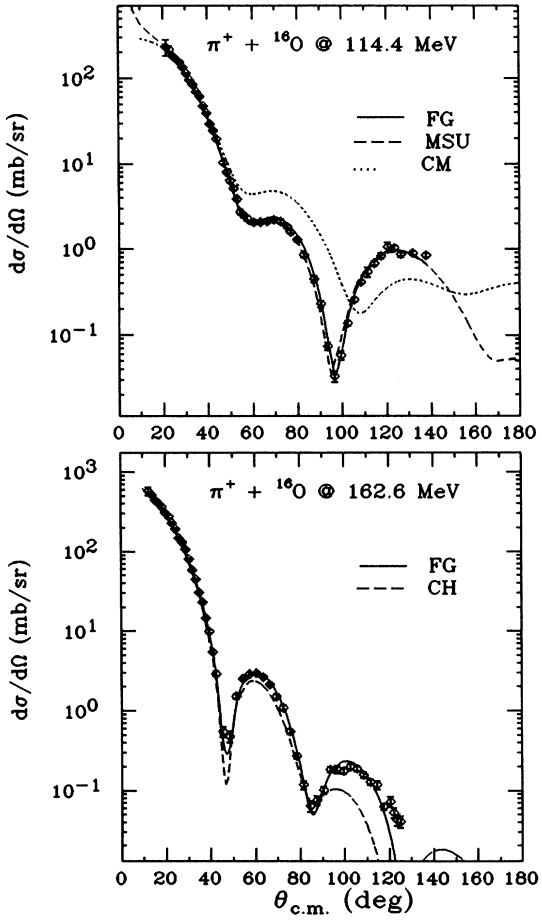

FIG. 5. Elastic scattering of π^+ from ^{16}O at 114.4 MeV and 162.6 MeV [9]. The curves represent optical model fits and are discussed in the text. The parameters are given in Table I. The solid curve (FG) represents the fixed geometry fit applied in the present analysis.

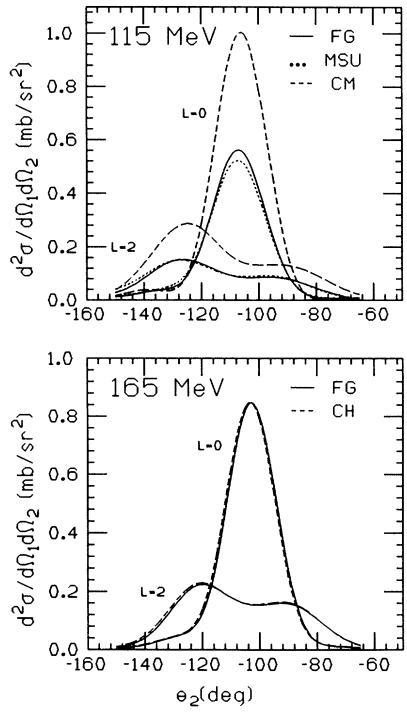

FIG. 6. DWIA calculations of the ^{16}O$(\pi^+, 2p)$ angular correlations using different optical model potentials discussed in the text. The calculations are for absorption on $L = 0$ and $L = 2$ deuterons with one proton at $\theta_1 = 50°$ and the second at angle θ_2. We have integrated over the momenta p_1 of the outgoing protons. The various curves are labeled by the pion optical potential with the solid curve (FG) representing the fixed geometry fit applied in the present analysis.

arise from deficiencies in the nuclear structure or from the reaction dynamics. However, in the present paper the DWIA calculations are used primarily as a method of determining the shape of the cross section, and not the absolute magnitude, in order to extrapolate the data into the unmeasured regions. Given the rather good description of the dependence of the experimental data on kinematic variables, the calculations should be adequate for extrapolation purposes. Additionally, and of great importance, we use the DWIA calculations to quantify the effects of FSI's by comparing calculations with and without an imaginary potential for the outgoing protons. The procedure and justification have been presented in some detail in our previous publication [5]. The results are primarily dependent on the proton optical model potential, and this is sufficiently well determined to provide a reliable estimate of the FSI.

B. Monte Carlo calculation of phase space distributions

There exists no theoretically based model for calculating the more complicated reaction processes which lead to four- or more-body final states. These processes can be of various types. For example, one can have an ISI in which the incoming pion knocks out a nucleon and then is absorbed on a pair of nucleons through a two-body absorption process. In a similar fashion one can have two-nucleon absorption followed by the knockout of additional nucleons by the outgoing protons (FSI). Beyond these more mundane processes which are part of the two-nucleon absorption process, multinucleon absorption by more than two nucleons in the nucleus may be possible. Such potentially interesting processes will populate the same kinetic regions, and without detailed theoretical calculations, or at least theoretical guidance, will be difficult to extract. This is especially true in an experiment in which only two final state protons are detected. We make no attempt to extract these multinucleon processes in this work. Rather we want a model which will allow us to subtract such processes from our data, independent of their origin, in order that we may extract a total direct two-nucleon absorption cross section.

Following the works of Refs. [1, 4, 23], in which three-nucleon final state experimental data were analyzed, we have chosen to simulate the multinucleon "background" using phase space. In particular, we assume uniform population of four-body phase space (three nucleons and the residual mass 13 nucleus), subject to a weighting which restricts the momentum of the residual nucleus to a Gaussian momentum distribution with width $\sigma = \sigma_0\sqrt{3}$ MeV/c. Such calculations constitute a spectator model in which the motion of a group of three nucleons in the initial ^{16}O nucleus is assumed to be described by a Gaussian momentum distribution, and the incoming pion is absorbed by the three nucleons.

Although this is an exceedingly simplified model, it, along with the DWIA, provides a good description of the present data. This model also describes ^{3}He$(\pi^+, 2p)$ data in regions of phase space far from those dominated by the two-nucleon absorption process [24]. We have therefore adopted this simple model as a method of providing a description of the multinucleon "background" processes, independent of their origin.

The calculations were carried out with the Monte Carlo code FOWL [25]. The geometry of our experimental setup was incorporated, and simulations done for four-body (three-nucleon) phase space. The width parameter of the Gaussian momentum distribution σ_0 was chosen by comparing calculations to the two-nucleon absorption data. In this case the pions were assumed to be absorbed on a nucleon pair which had a Gaussian momentum distribution of width $\sigma_0\sqrt{2}$ relative to the residual nucleus. The size parameter σ_0 was varied until a reasonable description of the width of the angular correlation data was obtained. The value was $\sigma_0 = 80$ MeV/c.

Comparisons of the two sets of calculations, DWIA and phase space simulations, with the data are presented in the next section.

V. TWO-NUCLEON ABSORPTION CROSS SECTIONS

In this section we compare the results of the two calculations to the experimental data, and extract the two-nucleon absorption cross section for the different excitation energy regions and the two incident energies. We have chosen initially to compare the calculations to data with minimum granularity. Therefore, the momentum sharing distributions of Figs. 3 and 4 have been integrated to generate a single differential cross section $(d\sigma/d\Omega_1)$ with the acceptance of the experiment for each angle θ_1 and each set of data. Such data we shall refer to as an angular distribution. Note that the data affected by the plastic scintillator threshold were excluded from the integral.

One can see how such angular distributions might be less sensitive than the momentum sharing distributions to the details of the theoretical model. If quasideuteron two-nucleon absorption was dominant and the experiment had 100% acceptance for $(\pi^+, 2p)$, the quantity $d\sigma/d\Omega_1$ would be essentially the $\pi^+ d \rightarrow pp$ differential cross section (neglecting small effects due to three-body phase space and the Fermi motion). This statement would be true independent of the relative contributions from different angular momentum transfer, e.g., $L = 0$ and $L = 2$ for the low excitation energy region. On the other hand, the momentum sharing distribution more closely reflects the momentum distribution of the bound deuteron, and as such is rather sensitive to the mixture of angular momentum transfer. Similarly, the angular distributions for the phase space calculations will be less sensitive to the detailed momentum distribution of the three-nucleon cluster. The phase space angular distributions discussed above are quite flat, and changes in details such as the width parameter σ_0, or even the number of particles in the final state, have rather little effect.

The single differential cross sections for the 0–20 MeV excitation energy range are shown in Figs. 7(a) (115 MeV) and 8(a) (165 MeV). Also shown is the shape of the free $\pi^+ d \rightarrow pp$ cross sections. The comparisons clearly show the effects of the limited acceptance of the present

experiment. For a fixed spectrometer angle θ_1 the associated proton from two-nucleon absorption populates a cone, centered at the $\pi^+ d \rightarrow pp$ conjugate angle, which is detected by our large scintillator array. When θ_1 is large the associated cone which goes to forward angles is relatively small, since the forward going proton has large momentum. Our detector accepts most of these events ($\sim$ 80%) with a single central setting. However, when θ_1 is small, the inverse is true and the central setting of the array captures only about 60% of the associated particles. (For the higher excitation energy the cone is larger due to the fact that the Fermi momentum is larger for more tightly bound particles.) The integrated quasideuteron absorption DWIA calculations for our experimental acceptance are also shown in Figs. 7(a) and 8(a). We see that with a single normalization the DWIA calculations reproduce the data quite well.

To extract the two-nucleon absorption cross section from these data, we first make the assumption that the shape of the angular distribution for two-nucleon absorption is the same as that for $\pi^+ d \rightarrow pp$. Second, we assume that backgrounds due to more complicated processes can be represented by our phase space Monte Carlo simulations, and have integrated them over the experimental acceptance to generate $d\sigma/d\Omega_1$ (background). Third, we obtain an extrapolation factor for each angle from the DWIA calculations by taking the ratio of the DWIA cross section integrated over the acceptance of our experiment to the DWIA cross section integrated over the entire phase space.

The procedure is then iterative. For each excitation energy we first subtract the simulated multinucleon background, normalized with a particular constant, from the

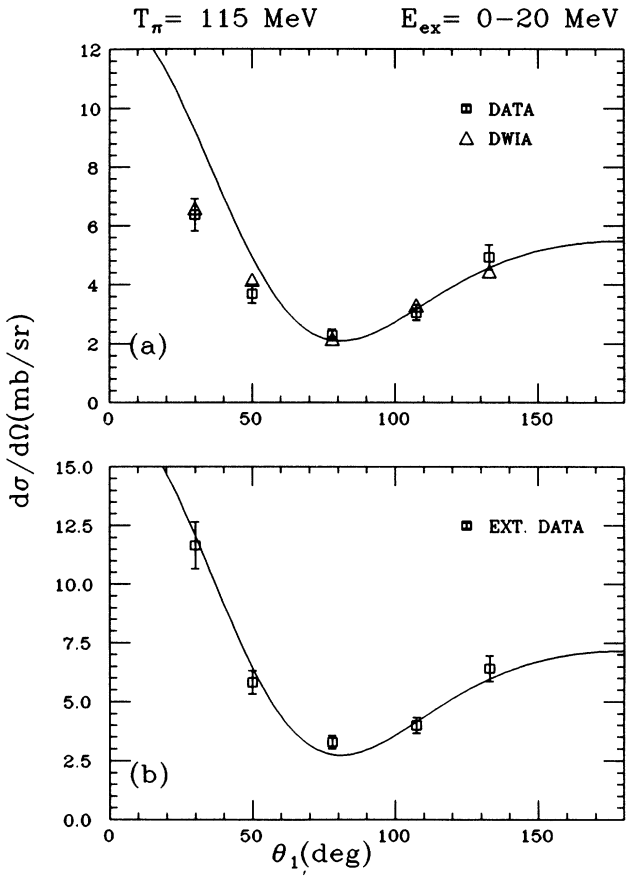

FIG. 7. Angular distributions at T_π = 115 MeV and E_{ex} = 0–20 MeV obtained by integrating over the second proton. (a) The data (□) represent the integral of the momentum sharing distributions (up to the onset of the plastic scintillator threshold) presented in Fig. 3. The triangles represent the integral of the DWIA calculations with the same limits as the experimental data and normalized to the momentum sharing distributions as displayed in Fig. 9. The curve represents the $\pi^+ d \rightarrow pp$ cross section [13] at 115 MeV arbitrarily normalized. (b) The squares represent the data of panel (a) extrapolated into the unmeasured regions using the DWIA calculations. The curve represents the $\pi^+ d \rightarrow pp$ cross section at 115 MeV normalized to the data.

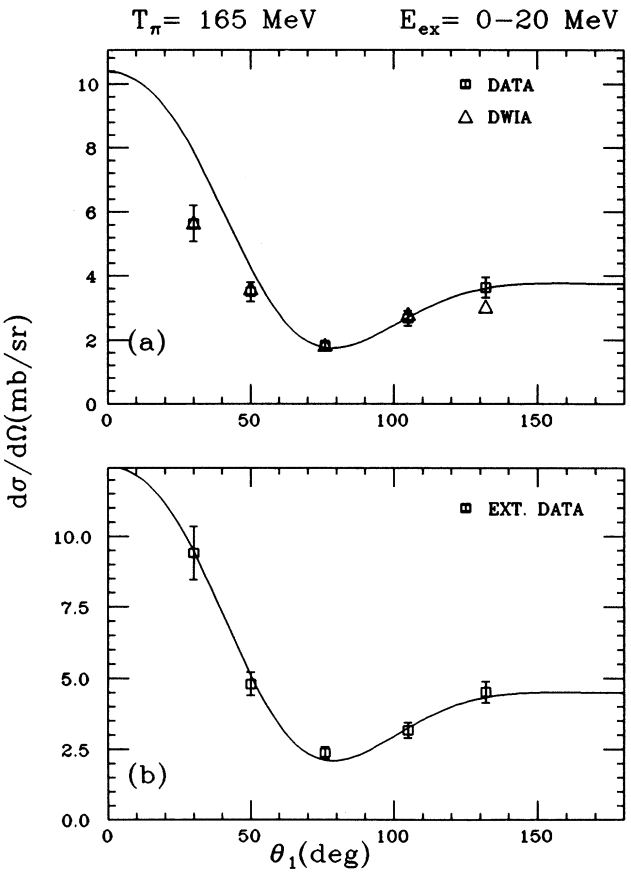

FIG. 8. Angular distributions at T_π = 165 MeV and E_{ex} = 0–20 MeV obtained by integrating over the second proton. (a) The data (□) represent the integral of the momentum sharing distributions presented in Fig. 3. The triangles represent the integral of the DWIA calculations normalized to the momentum sharing distributions as displayed in Fig. 10. The curve represents the $\pi^+ d \rightarrow pp$ cross section [13] at 165 MeV arbitrarily normalized. (b) The squares represent the data of panel (a) extrapolated into the unmeasured regions using the DWIA calculations. The curve represents the $\pi^+ d \rightarrow pp$ cross section at 165 MeV normalized to the data.

experimental angular distribution data. We then multiply the difference by the extrapolation factors determined from the DWIA calculations. The resultant angular distribution is compared to the shape of the free $\pi^+ d \rightarrow pp$ cross section and the process repeated, varying the background normalization constant, until the resultant is well described by the $\pi^+ d \rightarrow pp$ differential cross section.

A. Direct two-nucleon absorption (0–20 MeV)

The results of this procedure for the 0–20 MeV region are shown in Figs. 7(b) and 8(b). In this case the normalization of the background was consistent with zero for both incident energies. We thus conclude that this region is primarily populated by direct two-nucleon absorption. This is not too surprising considering the fact that the bulk of the yield lies at excitation energies below the breakup threshold of ^{14}N, and that according to shell model calculations essentially all of the $(1p)^2$ strength lies in this energy region.

The total cross sections are then obtained by integrating the normalized $\pi^+ d \rightarrow pp$ differential cross section shown in Figs. 7(b) and 8(b). The resulting cross sections are presented in the first column of Table II. These represent the directly measured two-nucleon absorption cross sections for 0–20 MeV excitation in ^{14}N with no ISI or FSI corrections. The errors reflect the statistical and systematic errors of the present experiment. The effects of the FSI are included in the next subsection.

Having completed the analysis of the angular distribution data, we show a more detailed comparison in Figs. 9 and 10, where we have compared the DWIA calculations directly to the momentum sharing distributions. The comparisons of the calculations to these data were actually done in parallel with the analysis of the angular distribution data, since due to the limited acceptance of the experiment the mixture of the two angular momenta has a small, but non-negligible, effect on the angular distribution analysis. The choice of the normalizations for the $L = 0$ and $L = 2$ DWIA calculations was done as in the previous analyses [5, 6, 12] by first fitting data for a

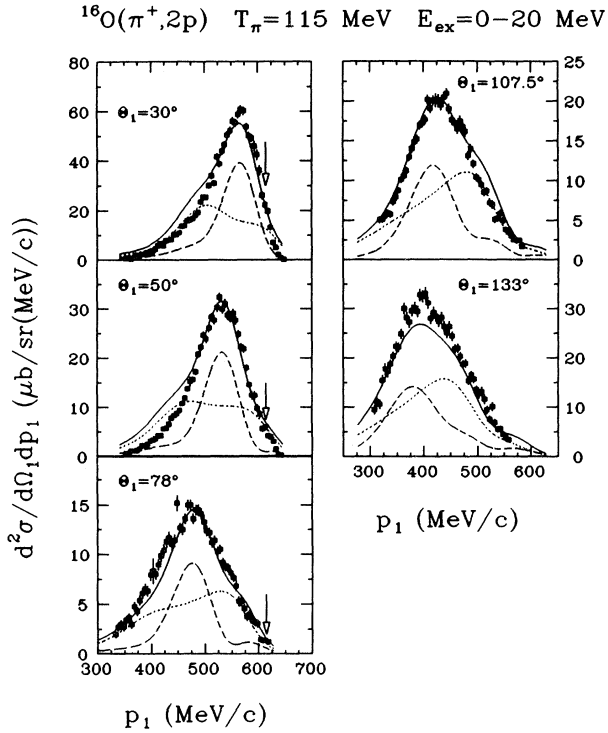

FIG. 9. Momentum sharing distributions as in Fig. 3 for the ^{16}O(π^+, 2p)^{14}N reaction at T_π = 115 MeV and with E_{ex} = 0–20 MeV. The curves are the normalized DWIA for $L = 0$ (dashed curve) $L = 2$ (dotted curve), and their sum (solid curve). The downward arrows indicate the onset of the plastic scintillator threshold. Data above this point represent lower limits.

TABLE II. 115 MeV and 165 MeV quasideuteron absorption cross sections for each missing mass region. The unperturbed experimental cross section (direct), the yield obtained after corrections, and the fraction of the total absorption cross section[a] σ_{abs} are listed.

	Direct σ (mb)	% of σ_{abs}	σ corrected[b] for FSI's (mb)	% of[b] σ_{abs}
0–20 MeV				
115 MeV	35±3	17±3	87±7	42±8
165 MeV	28±2	15±3	61±5	33±7
20–70 MeV				
115 MeV	245±5	12±3	64±12	31±7
165 MeV	13±2	7±2	33±6	18±5
20–45 MeV				
165 MeV	8.6±1.5	4.6±1.2	22±4	11.5±3.0
45–70 MeV				
165 MeV	4.6±0.8	2.4±0.6	11±2	6.1±1.6
0–70 MeV				
115 MeV	60±5	29±5	152±14	74±14
165 MeV	41±3	22±5	94±8	50±10

[a] σ_{abs} = 206 ± 33 mb at 115 MeV, 188 ± 36 mb at 165 MeV [36].

[b] The quoted errors exclude the error due to the final state interaction correction which is estimated to be 15%–20% (see text).

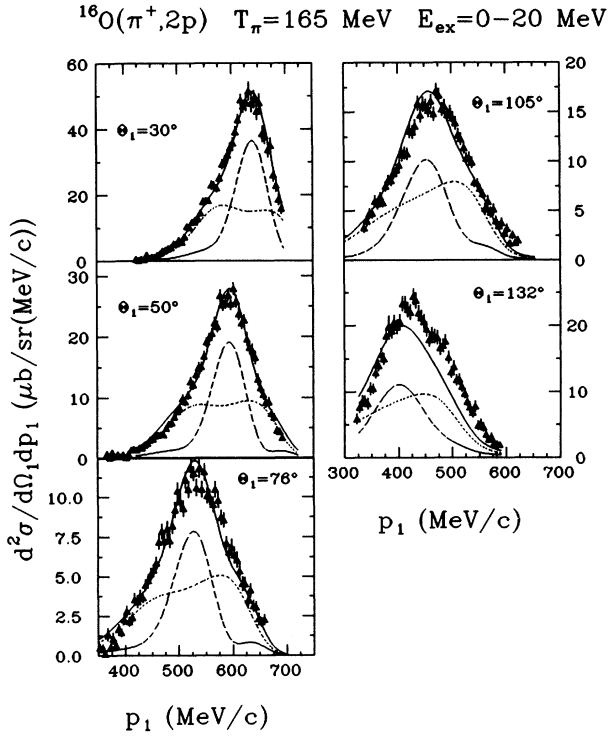

FIG. 10. Momentum sharing distributions as in Fig. 3 for the $^{16}O(\pi^+,2p)^{14}N$ reaction at T_π = 165 MeV and with E_{ex} = 0–20 MeV. The curves are the normalized DWIA for L = 0 (dashed curve) L = 2 (dotted curve), and their sum (solid curve). The data are unaffected by the the plastic scintillator threshold.

9° × 9° cut on the plastic array centered at the quasifree angle. In this case the peak yield arises predominantly (>90%) from the L = 0 states. Once this normalization had been obtained, the normalization of the L = 2 calculation was chosen by obtaining the best overall description of the momentum sharing data. These calculations were then integrated and summed incoherently to obtain the DWIA angular distributions presented in Figs. 7(a) and 8(a). As can be seen in the figures, the DWIA calculations describe the 0–20 MeV excitation energy momentum sharing data very well. An interesting aspect is that the normalizations of the DWIA calculations as presented are identical for the two incident energies. We shall return to this point later.

B. Direct two-nucleon absorption (20–70 MeV)

The same procedure was followed for the 20–70 MeV excitation energy region. For the 165 MeV data this region was subdivided into two parts. In this excitation energy range contributions from multinucleon background are more visible. In Figs. 11(a), 12(a), and 13(a) we present the angular distributions extracted from the measured experimental data. In all cases the angular distributions are flatter than those for the 0–20 MeV range. This is particularly true of the 45–70 MeV excitation energy data at 165 MeV. Also shown in these figures (a) are the simulated multinucleon angular distributions with the final normalization resulting from our iterative procedure. In the second panels [Figs. 11(b), 12(b), and 13(b)] we present the angular distributions following subtraction of the multinucleon background. We note that the multinucleon background contribution is quite sizable at 165 MeV, particularly for the 45–70 MeV excitation energy region. However, at 115 MeV the background is more modest, representing only about 20% of the yield even at 78° where the absorption on a quasideuteron is a

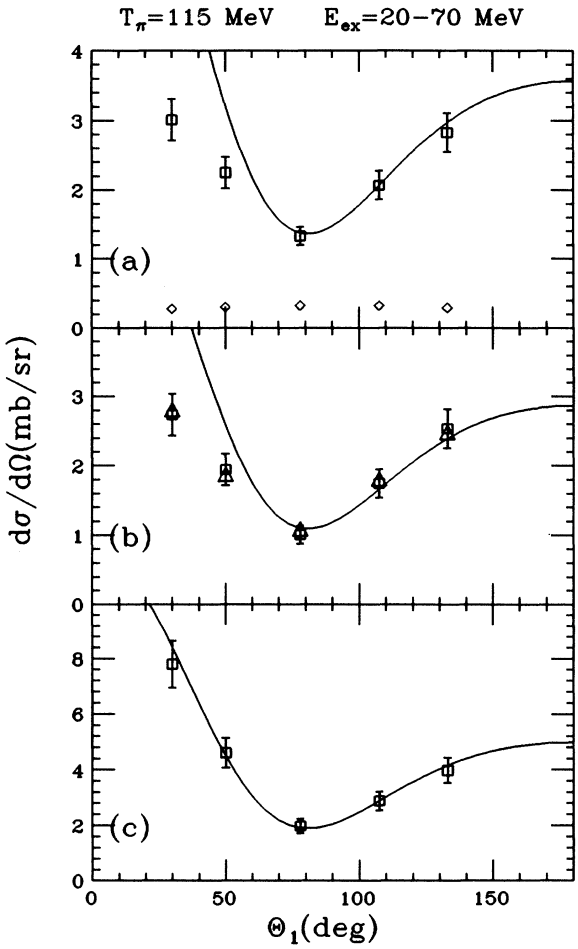

FIG. 11. Angular distributions at T_π = 115 MeV and with E_{ex} = 20–70 MeV obtained by integrating over the second proton. In each panel the curve represents the $\pi^+ d \rightarrow pp$ cross section [13] at 115 MeV normalized to the data. (a) The data (□) represent the integral of the experimental momentum sharing distributions (up to the onset of the plastic scintillator threshold) presented in Fig. 4. The diamonds represent the integral of the four-body phase space calculations normalized as discussed in the text. (b) The squares represent the difference between the data and the phase space calculations as presented in panel (a). The triangles represent the integral of the DWIA calculations normalized to the momentum sharing distributions as displayed in Fig. 14. (c) The squares represent the data of panel (b) extrapolated into the unmeasured regions using the DWIA calculations.

minimum. Also shown in these panels (b) are the DWIA calculations for $(1s\text{-}1p)$ $L = 1$ integrated over the detector acceptance.

The bottom panels [Figs. 11(c), 12(c), and 13(c)] present the final angular distributions, after multiplying by the extrapolation factors determined from the DWIA calculations. Note that the extrapolations are larger for this excitation energy region due to the fact that the angular correlation is broader as has been discussed.

The integrated two-nucleon absorption yield, using the $\pi^+ d \rightarrow pp$ angular distribution as before, is presented in the first column of Table II. In this case an error reflecting a 50% variation in the subtracted background has been taken in quadrature with the systematic errors for each cross section.

Again to provide a more detailed comparison the momentum sharing distributions are compared to the theoretical calculations in Figs. 14, 15, and 16. At both incident energies we obtain a rather good fit to the data by including a multinucleon background. The magnitudes, shapes, and angular dependence of the cross sections are quite well described.

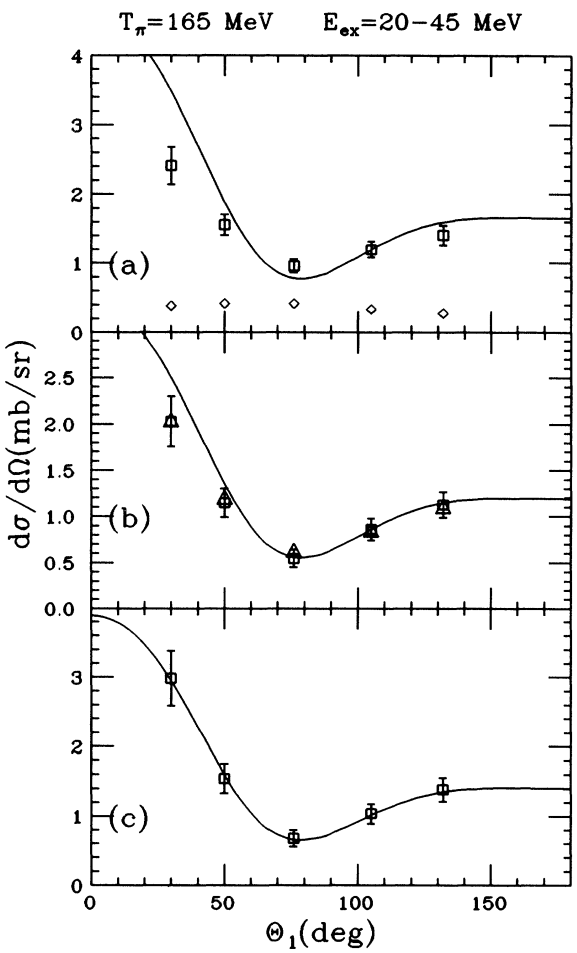

FIG. 12. Angular distributions at $T_\pi = 165$ MeV and with $E_{ex} = 20$–45 MeV obtained by integrating over the second proton. In each panel the curve represents the $\pi^+ d \rightarrow pp$ cross section [13] at 165 MeV normalized to the data. (a) The data (□) represent the integral of the experimental momentum sharing distributions (up to the onset of the plastic scintillator threshold) presented in Fig. 15. The diamonds represent the integral of the four-body phase space calculations normalized as discussed in the text. (b) The squares represent the difference between the data and the phase space calculations as presented in panel (a). The triangles represent the integral of the DWIA calculations normalized to the momentum sharing distributions as displayed in Fig. 15. (c) The squares represent the data of panel (b) extrapolated into the unmeasured regions using the DWIA calculations.

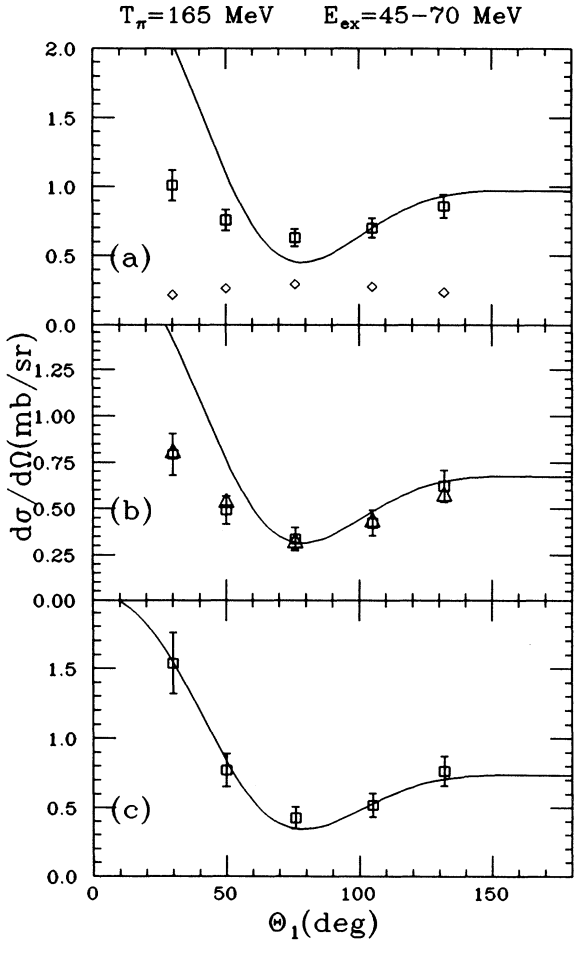

FIG. 13. Angular distributions at $T_\pi = 165$ MeV and with $E_{ex} = 45$–70 MeV obtained by integrating over the second proton. In each panel the curve represents the $\pi^+ d \rightarrow pp$ cross section at 165 MeV normalized to the data. (a) The data (□) represent the integral of the experimental momentum sharing distributions (up to the onset of the plastic scintillator threshold) presented in Fig. 16. The diamonds represent the integral of the four-body phase space calculations normalized as discussed in the text. (b) The squares represent the difference between the data and the phase space calculations as presented in panel (a). The triangles represent the integral of the DWIA calculations normalized to the momentum sharing distributions as displayed in Fig. 16. (c) The squares represent the data of panel (b) extrapolated into the unmeasured regions using the DWIA calculations.

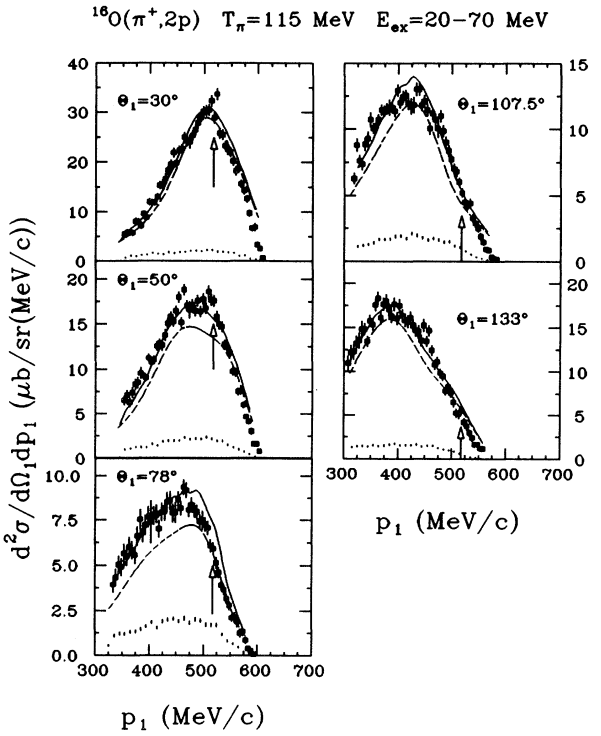

FIG. 14. Momentum sharing distributions as in Fig. 4 for the $^{16}O(\pi^+, 2p)^{14}N$ reaction at T_π = 115 MeV and with E_{ex} = 20–70 MeV. The dashed curves are the normalized DWIA for L = 1. The vertical bars are Monte Carlo four-body phase space simulations, the height representing the statistical error, normalized as in Fig. 11. The solid curve is the smoothed sum of the two calculations. The arrows indicate the onset of the plastic scintillator threshold. Data above this point represent lower limits.

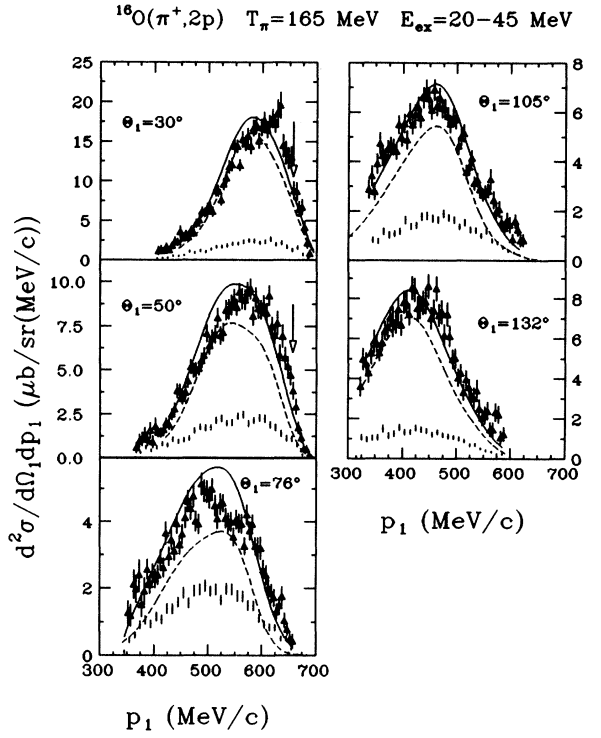

FIG. 15. Momentum sharing distributions for the $^{16}O(\pi^+, 2p)^{14}N$ reaction at T_π = 165 MeV and with E_{ex} = 20–45 MeV. The dashed curves are the normalized DWIA for L = 1. The vertical bars are Monte Carlo four-body phase space simulations, the height representing the statistical error, normalized as in Fig. 12. The solid curve is the smoothed sum of the two calculations. The arrows indicate the onset of the plastic scintillator threshold. Data above this point represent lower limits.

C. Total direct two-nucleon absorption

The first column of Table II contains the cross sections extracted directly from the experimental data. The measured direct two-nucleon absorption cross section represents about 29% of the total absorption cross section at 115 MeV, dropping to about 22% at 165 MeV. Thus, our more detailed analysis agrees with the qualitative conclusions reached in Sec. III concerning the energy dependence of the two-nucleon absorption cross section. There we noted that both the inclusive and exclusive cross sections fell with energy more rapidly than the $\pi^+ d \rightarrow pp$ cross section.

D. Final state interactions: total two-nucleon absorption cross sections

The data presented in the first two columns of Table II represent the direct two-nucleon absorption cross section. As discussed in the Introduction, one can also have two-nucleon absorption either preceded (ISI) or followed (FSI) by additional interactions. For the latter we believe that the DWIA, combined with a good phenomenological proton optical model potential, provides a satisfactory method of calculating the effects of final state interactions on the two-nucleon absorption process. A detailed discussion of this FSI correction is given in Ref. [5]. Briefly, we have carried out a series of DWIA calculations of two-nucleon absorption both with and without the imaginary part of the proton optical model potential. We assume that the ratio of the calculations with no proton imaginary potential to those with the proton imaginary potential represents the effect of FSI's on the magnitude of the two-nucleon absorption cross section. The same type of calculation, also using the Nadasen *et al.* [17] proton optical model potential, is capable of predicting the ratio of the $(e, e'p)$ exclusive cross sections to (e, e') inclusive cross sections to within about 15% for a range of nuclei from ^{12}C to ^{181}Ta [26, 27]. Further discussion supporting this treatment of FSI's is presented in Ref. [5].

In the calculations we find the FSI correction factor for the 0–20 MeV excitation region to be large (approximately 2.5 at 115 MeV and 2.2 at 165 MeV) and to be almost independent of the angle θ_1 (<10% variation). The correction is somewhat larger for the 20–70 MeV

excitation energy region and for $L > 0$ ($\lesssim 10\%$). Note that although the FSI correction factor appears to be very large, it corresponds to a correction of about 1.5–1.6 for each final state proton. This in turn implies only about a 35% chance that the outgoing proton undergoes an inelastic collision with the residual nucleus.

We have multiplied the extracted direct two-nucleon absorption cross sections presented in Table II by the appropriate calculated DWIA ratios. The results, the total two-nucleon absorption cross section including FSI's, are presented in the last two columns of Table II. The error in the two-nucleon absorption cross section reflects the experimental error and an estimate of the error in the multinucleon "background" subtraction. However, no estimate of the error in the FSI correction is included.

The FSI corrections are very large and obviously have a major impact on our interpretation of the overall dominance of two-nucleon absorption in pion absorption on nuclei. Fortunately, we have available a reasonable test of our method of determining the FSI. In particular, for regions of phase space dominated by two-nucleon absorption, we can compare the inclusive and exclusive cross sections. In terms of FSI's the difference in the magnitudes of the two cross sections is primarily due to the FSI of one of the outgoing protons. Thus, in our DWIA model, if the FSI treatment is adequate, we should be able to calculate the inclusive cross sections (in regions dominated by two-nucleon absorption) for each angle θ_1. This is done by using the normalizations obtained from the analysis of the exclusive data, setting the imaginary part of the optical model potential for the second proton equal to zero, and integrating the DWIA calculation over the full angular range of the second proton.

The results of these calculations are presented in Figs. 17 and 18. For consistency in the analysis we have also included our multinucleon simulation, which we would like to normalize as in the analysis of the exclusive data. This, however, is difficult since it is necessary to choose the nucleon content (protons or neutrons) of the three nucleons absorbing the pion. Based on the three-nucleon final state data of Ransome *et al.* [3], we have assumed the dominance of absorption on (*pnn*) triplets leading to a (*ppn*) final state. Because of the uncertainty, we believe that the comparison to the inclusive data is most valid at 30°, where the two-nucleon cross section is large, and the multinucleon cross section is relatively small. Here we see that at both energies the peak cross section is underpredicted by only about 10–15%. When one considers

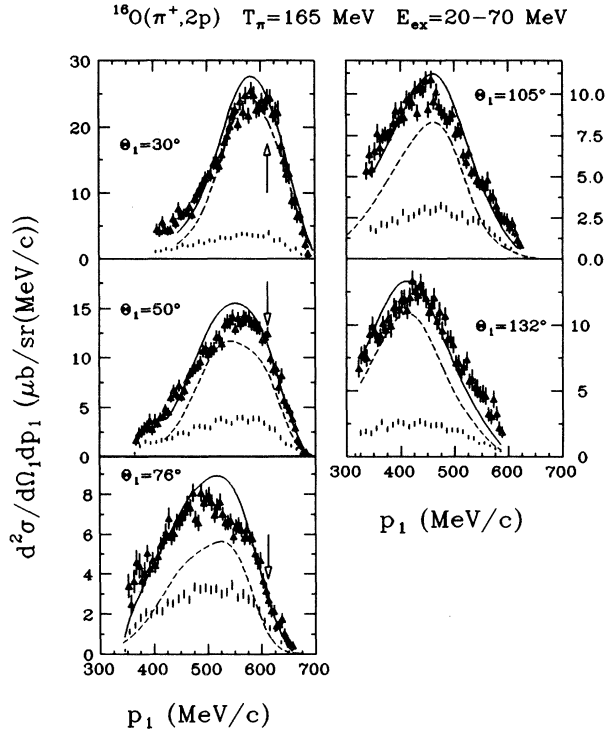

FIG. 16. Momentum sharing distributions for the $^{16}O(\pi^+, 2p)^{14}N$ reaction at T_π = 165 MeV and with E_{ex} = 20–70 MeV. The dashed curves are the normalized DWIA for L = 1. The vertical bars are Monte Carlo four-body phase space simulations, the height representing the statistical error, normalized as in Figs. 12 and 13. The solid curve is the smoothed sum of the two calculations. The arrows indicate the onset of the plastic scintillator threshold. Data above this point represent lower limits.

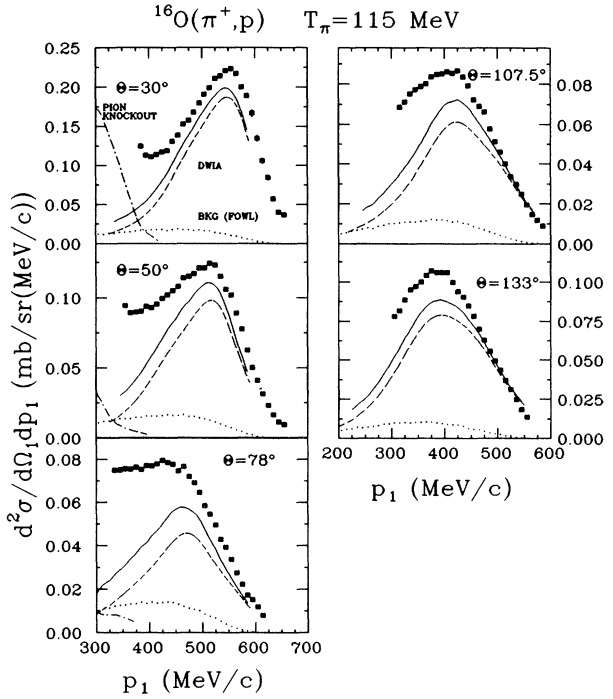

FIG. 17. Inclusive $^{16}O(\pi^+, p)$ cross sections (□) for an incident pion energy of 115 MeV as in Fig. 1. The dashed curves are the sum of the DWIA calculations for $L = 0$, $L = 1$, and $L = 2$ normalized to the momentum sharing distribution. The dotted curves represent the phase space simulations normalized as discussed in the text. The solid curve is the sum of the two calculations. For small angles the dot-dashed line represents a DWIA calculation for the $(\pi^+, \pi^+ p)$ reaction normalized to coincident data gated on pion events in the plastic scintillator array [8].

the contributions from (π^+, pn) two-nucleon absorption ($\lesssim 5\%$) [28] and other three-body final state absorption channels such as (π^+, pd) [23], the agreement is good. We therefore argue that our method for correcting the two-nucleon absorption cross section for the effects of FSI's is reliable, and probably accurate at the 15%–20% level.

Taking our FSI corrections we conclude that at 115 MeV the two-nucleon absorption process is dominant, a conclusion reached in our previous analysis. Including the (π^+, pn) channel the two-nucleon absorption with FSI's accounts for approximately 80% of the total absorption cross section. However, near the peak of the Δ resonance at 165 MeV, the fraction of the total absorption cross section contained in two-nucleon absorption corrected for FSI's drops to about 50%.

E. Comparison to theoretical predictions

The total cross section results are summarized in Fig. 19, where we have plotted the energy dependence of the direct two-nucleon absorption cross section, the total two-nucleon absorption cross section including FSI's, and the ratio of this to the total absorption cross section. The ratios at 115 and 165 MeV in Fig. 19(c) have been increased by 4% to account for undetected yield arising from (π^+, pn) reactions [28]. For completeness we have also included the results at 65 MeV [23, 29, 30]. In spite of the large errors, arising in part from the measured total absorption cross section, we see a systematic decrease in the fraction of the total absorption cross section which is two-nucleon absorption as the incident energy increases.

The calculations of Masutani and Yazaki [31] for ^{16}O and of Oset, Futami, and Toki [32] for ^{12}C are in remarkably good agreement with these results [see Fig. 19(c)]. In the calculations of Masutani and Yazaki, the losses from the two-nucleon channel are explicitly attributed to one or more pion initial state interactions (ISI's). Oset, Futami, and Toki attribute the losses to sequential Δ production, also ISI's. Although the DWIA calculations discussed in Sec. IV have to be normalized to the data, the normalization is the same at the two energies; this is also consistent with the increased losses from the two-nucleon channel at 165 MeV being due to ISI's, described by the pion potential. However, the attribution of large losses from the two-nucleon channel to ISI's is not consistent with experimental results [33, 34]. Indeed, the

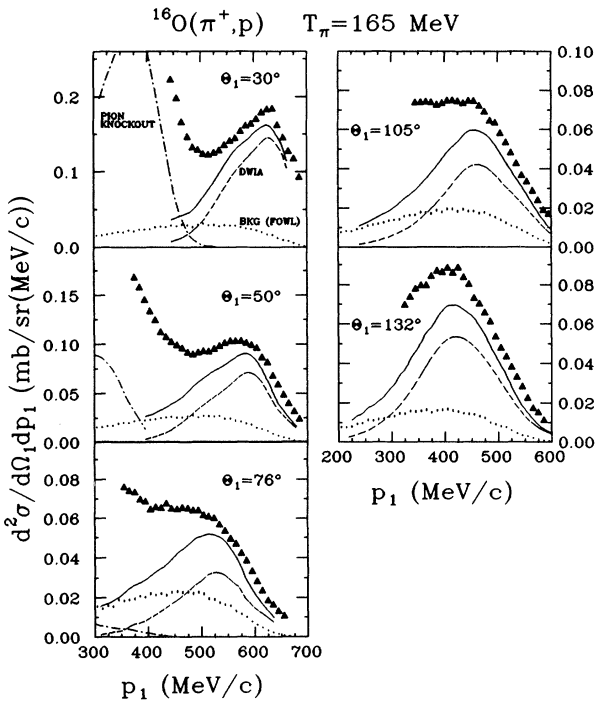

FIG. 18. Inclusive ^{16}O(π^+, p) cross sections ($\triangle$) for an incident pion energy of 165 MeV as in Fig. 1. The dashed curves are the sum of the DWIA calculations for $L = 0$, $L = 1$, and $L = 2$ normalized to the momentum sharing distribution. The dotted curves represent the phase space simulations normalized as discussed in the text. The solid curve is the sum of the two calculations. For small angles the dashed-dot line represents a DWIA calculation for the $(\pi^+, \pi^+ p)$ reaction normalized to the coincident data gated on pion events in the plastic scintillator array [8].

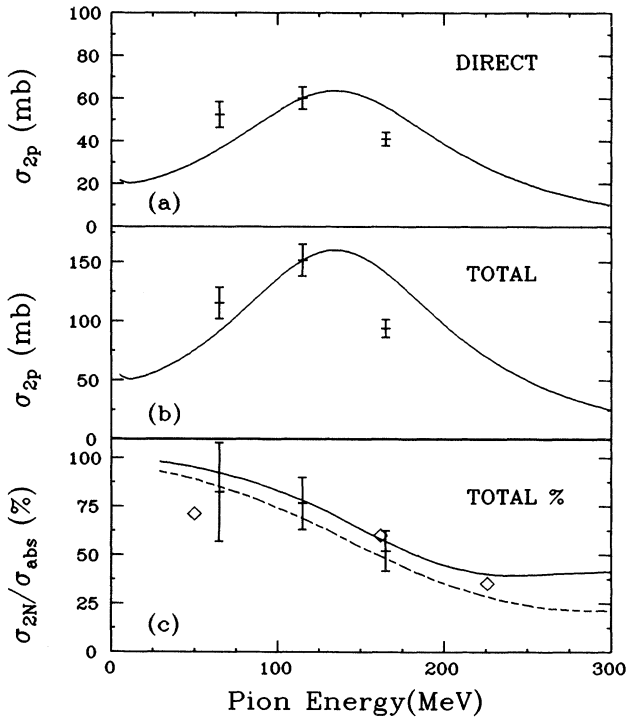

FIG. 19. Total two-nucleon absorption cross sections from the present experiment and that of Refs. [23, 29, 30]. (a) Direct two-nucleon absorption cross section. The curve represents the shape of the the $\pi^+ d \rightarrow pp$ total cross section. (b) Two-nucleon absorption cross section corrected for FSI's. (c) Ratio of total two-nucleon absorption cross section of panel (b) to the total absorption cross section. The curves represent calculations for ^{12}C with (dashed curve) and without (solid curve) medium modifications [32]. The diamonds ($\diamond$) represent calculations by Masutani and Yazaki [31].

absence of experimental evidence of ISI's before absorption is often taken as evidence to indicate that the losses must be due to multinucleon absorption dynamics. Since two-step pion quasifree scattering is quite strong, the apparent weakness of them in absorption is very puzzling [35].

VI. SUMMARY AND CONCLUSIONS

From measured $^{16}O(\pi^+, 2p)$ data covering a large fraction of the two-nucleon absorption phase space, we have extracted the direct two-nucleon absorption cross sections. These were extracted using a combination of DWIA calculations to describe the two-nucleon absorption, and four-body final state phase space calculations to describe multinucleon absorption or other more complicated processes. The combination of these calculations provides a good description of the shape of the experimental data, and therefore provides a good method of extrapolating the data into the unmeasured regions. The directly measured two-nucleon absorption cross sections are found to decrease more rapidly with energy than the $\pi^+ d \rightarrow pp$ cross section.

Using the DWIA we make quantitative predictions of the effects of FSI's on the two-nucleon absorption cross section. Although these are large, they are subject to test by comparing DWIA calculations to the inclusive $^{16}O(\pi^+, p)$ data. This comparison gives us confidence in the FSI corrections applied in this paper, and leads to the conclusion that two-nucleon absorption dominates at 115 MeV, decreasing to about 50% of the total absorption cross section at 165 MeV.

Finally, the energy dependence of the ratio of the two-nucleon to the total absorption cross section is described well by the calculations of Refs. [31] and [32] as well as those using the DWIA described here. However, all these calculations attribute the energy dependence to an increased pion ISI probability at the higher energy, in apparent contradiction to experimental searches for this process.

ACKNOWLEDGMENTS

This work was supported in part by the National Science Foundation and the U.S. Department of Energy. The authors gratefully acknowledge the extensive support of the PSI laboratory and staff during this experiment.

[1] R. Tacik, E. T. Boschitz, W. Gyles, W. List, C. R. Otterman, M. Wessler, U. Wiedner, and R. R. Johnson, Phys. Rev. C **40**, 256 (1989).
[2] H. J. Weyer, Phys. Rep. **195**, 295 (1990).
[3] R. D. Ransome, V. R. Cupps, S. Dawson, R. W. Fergerson, A. Green, C. L. Morris, J. A. McGill, J. R. Comfort, B. G. Ritchie, J. R. Tinsley, J. D. Zumbro, R. A. Loveman, P. C. Gugelot, D. W. Watson, and C. Fred Moore, Phys. Rev. C **42**, 1500 (1990).
[4] R. D. Ransome, C. L. Morris, M. K. Jones, B. G. Ritchie, D. L. Watson, J. A. McGill, K. Pujara, D. B. Clayton, I. Brown, P. Campbell, and C. Fred Moore, Phys. Rev. C **46**, 273 (1992).
[5] D. J. Mack, P. G. Roos, H. Breuer, N. S. Chant, S. D. Hyman, F. Khazaie, B. G. Ritchie, J. D. Silk, G. S. Kyle, P. A. Amaudruz, Th. S. Bauer, C. H. Q. Ingram, D. Renker, R. A. Schumacher, U. Sennhauser, and W. J. Burger, Phys. Rev. C **45**, 1767 (1992).
[6] S. D. Hyman, D. J. Mack, H. Breuer, N. S. Chant, F. Khazaie, B. G. Ritchie, P. G. Roos, J. D. Silk, P-A. Amaudruz, T. S. Bauer, C. H. Q. Ingram, G. S. Kyle, D. Renker, R. A. Schumacher, U. Sennhauser, and W. J. Burger, Phys. Rev. C **41**, R409 (1990).
[7] D. J. Mack, Ph.D. thesis, University of Maryland, 1987.
[8] Scott D. Hyman, Ph.D. thesis, University of Maryland, 1989.
[9] J. P. Albanese, J. Arvieux, J. Folger, E. Boschitz, C. H. Q. Ingram, J. Jansen, and J. Zichy, Nucl. Phys. **A350**, 301 (1980).
[10] P. G. Roos, L. Rees, and N. S. Chant, Phys. Rev. C **24**, 2647 (1981).
[11] N. S. Chant and P. G. Roos, Phys. Rev. C **39**, 957 (1989).
[12] R. A. Schumacher, P. A. Amaudruz, C. H. Q. Ingram, U. Sennhauser, H. Breuer, N. S. Chant, A. E. Feldman, B. S. Flanders, F. Khazaie, D. J. Mack, P. G. Roos, J. D. Silk, and G. S. Kyle, Phys. Rev. C **38**, 2205 (1988).
[13] B. G. Ritchie, Phys. Rev. C **44**, 533 (1991).
[14] Dahai Zhang, Ph.D. thesis, University of Maryland, 1990.
[15] S. Cohen and D. Kurath, Nucl. Phys. **A141**, 145 (1970).
[16] M. Gouweloos and M. Thies, Phys. Rev. C **35**, 631 (1987).
[17] A. Nadasen, P. Schwandt, P. P. Singh, W. W. Jacobs, A. D. Bacher, P. T. Debevec, M. D. Kaitchuck, and J. T. Meek, Phys. Rev. C **23**, 1023 (1981).
[18] J. F. Amman, P. D. Barnes, K. G. R. Doss, S. A. Dytman, R. A. Eisenstein, J. D. Sherman, and W. R. Wharton, Phys. Rev. C **23**, 1635 (1981).
[19] M. D. Cooper and R. A. Eisenstein, Los Alamos National Laboratory Report No. LA-5929-MS, 1975.
[20] J. A. Carr, H. McManus, and K. Stricker-Bauer, Phys. Rev. C **25**, 952 (1982).
[21] M. Khandaker (private communication).
[22] W. B. Cottingame and D. B. Holtkamp, Phys. Rev. Lett. **45**, 1828 (1980).
[23] Th. S. Bauer, R. Hamers, P. Boberg, H. Breuer, R. van Dantzig, F. Geerling, S. Hyman, J. Konijn, C. T. A. M. de Laat, Y. Lefevere, A. Taal, J. L. Visschers, and R. Ykema, Phys. Rev. C **46**, R20 (1992).
[24] G. Backenstoss, M. Izycki, P. Salvisberg, M. Steinacher, P. Weber, H.J. Weyer, S. Cierjacks, S. Ljungfelt, H. Ullrich, M. Furie, and T. Petkovic, Phys. Rev. Lett. **55**, 2782 (1985).
[25] F. James, CERN Computer Center Program Library, W515 (1975).
[26] D. F. Geesaman, R. Gilman, M.C. Green, R.J. Holt, J.P. Schiffer, B. Zeidman, G. Garino, M. Saber, R. E. Segel, E. J. Beise, G. W. Dodson, S. Høibråten, L. D. Pham R. P. Redwine, W. W. Sapp, C. F. Williamson, S. A. Wood, N. S. Chant, P. G. Roos, J. D. Silk, M. Deady, and X. K. Maruyama, Phys. Rev. Lett. **63**, 734 (1989).

[27] G. Garino, M. Saber, R. E. Segel, D. F. Geesaman, R. Gilman, M. C. Green, R. J. Holt, J. P. Schiffer, B. Zeidman, E. J. Beise, G. W. Dodson, S. Høibråten, L. D. Pham, R. P. Redwine, W. W. Sapp, C. F. Williamson, S. A. Wood, N. S. Chant, P. G. Roos, J. D. Silk, M. Deady, and X. K. Maruyama, Phys. Rev. C **45**, 780 (1992).

[28] A. Altman, D. Ashery, E. Piasetzky, J. Lichtenstadt, A. I. Yavin, W. Bertl, L. Felawka, H. K. Walter, R. J. Powers, R. G. Winter, and J. v. d. Pluym, Phys. Rev. C **34**, 1757 (1986).

[29] Ronald Hamers, Ph.D. thesis, Vrije University, 1989.

[30] Remco Ykema, M.S. thesis, Universität van Amsterdam, 1989.

[31] K. Masutani and K. Yazaki, Nucl. Phys. **A407**, 309 (1983).

[32] E. Oset, Y. Futami, and H. Toki, Nucl. Phys. **A448**, 597 (1986).

[33] W. J. Burger, E. Beise, S. Gilad, R. P. Redwine, P. G. Roos, N. S. Chant, H. Breuer, G. Ciangaru, J. D. Silk, G. S. Blanpied, B. M. Preedom, B. G. Ritchie, M. Blecher, K. Gotow, D. M. Lee, and H. Ziock, Phys. Rev. C **41**, 2215 (1990).

[34] W. Brückner, H. Döbbeling, P. C. Gugelot, F. Güttner, H. Kneis, S. Majewski, M. Nomachi, S. Paul, B. Povh, R. D. Ransome, T. A. Shibata, M. Treichel, Th. Walcher, P. Amaudruz, Th. Bauer, J. Domingo, R. Frey, Q. Ingram, H. Jantzen, G. Kyle, D. Renker, and R. A. Schumacher, Nucl. Phys. **A469**, 617 (1987).

[35] C. H. Q. Ingram, in Proceedings of the International Nuclear Physics Conference, Wiesbaden, Germany, 1992 (in press).

[36] C. H. Q. Ingram, P. A. M. Gram, J. Jansen, R. E. Mischke, J. Zicky, J. Bolger, E. T. Boschitz, G. Pröbstle, and J. Arvieux, Phys. Rev. C **27**, 1578 (1983).